REPORT DOCUMENTATION PAGE

AFRL-SR-AR-TR-05-

0486

1. REPORT DATE *(DD-MM-YYYY)*	2. REPORT TYPE	3. DATES COVERED *(From - To)*
25-11-2005	Final Technical	01-01-2005 - 30-06-2005

4. TITLE AND SUBTITLE

(U) Experimental Study of Velocity-Conserved Scalar Filtered Joint Density Function for Improving Large Eddy Simulation Of Turbulent Combustion

5a. CONTRACT NUMBER

5b. GRANT NUMBER
F49620-02-1-0130

5c. PROGRAM ELEMENT NUMBER
61102F

6. AUTHOR(S)

Chenning Tong

5d. PROJECT NUMBER
2308

5e. TASK NUMBER
BX

5f. WORK UNIT NUMBER

7. PERFORMING ORGANIZATION NAME(S) AND ADDRESS(ES)

Department of Mechanical Engineering
Clemson University
Clemson SC 29634

8. PERFORMING ORGANIZATION REPORT NUMBER

9. SPONSORING / MONITORING AGENCY NAME(S) AND ADDRESS(ES)

AFOSR/NA
875 North Randolph Street
Suite 325, Room 3112
Arlington VA 22203-1768

10. SPONSOR/MONITOR'S ACRONYM(S)

11. SPONSOR/MONITOR'S REPORT NUMBER(S)

12. DISTRIBUTION / AVAILABILITY STATEMENT

Approved for public release; distribution is unlimited

13. SUPPLEMENTARY NOTES

14. ABSTRACT

The filtered mass density function (FMDF) of mixture fraction and other filtered variables used in large-eddy simulation of turbulent combustion were studied using measurement data obtained in turbulent partially premixed methane/air (Sandia) flames. For subgrid-scale (SGS) scalar variance small compared to its mean, the FMDF was not far from Gaussian, and the SGS scalar was well mixed. For large SGS variance, the FMDF became bimodal, and the conditionally filtered scalar dissipation was bell-shaped, indicating the existence of a diffusion (dissipation) layer structure, which was similar to the mixture fraction profile in the counter-flow model for laminar flamelets. The conditionally filtered temperature near the stoichiometric mixture fraction decreased progressively with increasing SGS scalar variance. Local extinction events appeared to occur mostly when the SGS scalar variance was large, suggesting the possibility of flamelet extinction. The results suggested that the mixing regimes and the associated mixture fraction structure potentially could potentially have strong influences on the combustion regime and extinction/reignition in turbulent nonpremixed flames.

15. SUBJECT TERMS

Turbulent combustion, large eddy simulation, joint probability density function, subgrid-scale modeling, flamelet

16. SECURITY CLASSIFICATION OF:			17. LIMITATION OF ABSTRACT	18. NUMBER OF PAGES	19a. NAME OF RESPONSIBLE PERSON
a. REPORT	b. ABSTRACT	c. THIS PAGE			Julian M. Tishkoff
Unclassified	Unclassified	Unclassified	UL	35	19b. TELEPHONE NUMBER *(include area code)* (703) 696-8478

Final Report: Experimental study of velocity-scalar filtered joint density function for improving large-eddy similation of turbulent combustion

AFOSR Grant F-49620-02-1-0130

Principal Investigator: Chenning Tong

Department of Mechanical Engineering
Clemson University
Clemson, SC 29634-0921

I Introduction

This research project focused on issues met in using large-eddy simulation (LES) to predict turbulent nonpremixed combustion. LES has been recognized as a very promising approach to modeling such flows[1, 2, 3]. In this approach the subgrid-scale (SGS) scalar mixing and the resulting instantaneous distribution of scalar values in each grid volume (i.e., the filtered density function) must be faithfully represented in order to accurately predict the chemical reaction rate. An important modeling method uses the transport equation of the filtered joint density function of velocity and scalars in which both the reaction source term and the turbulent transport terms are in closed form[3]. This research studied issues in using this approach by investigating the SGS mixing of conserved scalars which often play a crucial role in LES of nonpremixed combustion.

Significant progress has been made in understanding the SGS velocity and scalar filtered density function and their dynamics and issues of LES modeling. Specifically, the following work was completed:

- Proved Galilean invariance of the velocity probability density function (PDF), velocity filtered density function, their transport equations, and the statistics conditional on one-point velocity. The proof provides a formal justification of using the PDF-based approach to model turbulent flows in a manner that is invariant in any inertial reference frame.

- Investigated the filtered joint density function of velocity components (VFJDF) and its transport equation using experimental data. The VFJDF and the structure of the SGS velocity are found to strongly depend on to degree of nonequilibrium spectral transfer.
- Investigated the dependence of the structure of SGS velocity on the nonequilibrium spectral energy transfer. The results are important for establishing a framework for modeling the degree of nonequilibrium spectral transfer and the VFJDF.
- Investigated the filtered joint density function of velocity components and a conserved scalar (VSFJDF) and its transport equation using experimental data. The VSFJDF and the coupling between the SGS velocity and scalar are found to depend strongly on the degree of nonequilibrium spectral transfer.
- Investigated the dependence of the structure of SGS scalar fields on nonequilibrium spectral energy and scalar transfer. The dependence is important for establishing a framework for modeling the degree of nonequilibrium spectral transfer and the VSFJDF.
- Investigated the issues of modeling the filtered energy dissipation and the filtered scalar dissipation.
- Conducted a preliminary study of SGS mixing of the mixture fraction and the SGS flame structure. The study was based on the knowledge gained in the above-mentioned work, and the preliminary results have strong implications for studying SGS flame structure and local extinction and reignition.

The primarily findings of this research are discussed in the following.

II Nomenclature

$B = K - S^2$	bimodality parameter
f	(joint) probability density function (PDF, JPDF)
f_L	filtered (joint) density function (FDF, FJDF)
K	kurtosis
$k_L = (\langle u_1''^2 \rangle_L + \langle u_2''^2 \rangle_L)/2$	SGS kinetic energy
$k_r\ (= k_L)$	local kinetic energy

P	(joint) probability density function
$\mathcal{P}_{\phi r} = -(\langle u_j \phi \rangle_r - \langle u_j \rangle_r \langle \phi \rangle_r) \frac{\partial \langle \phi \rangle_r}{\partial x_j}$	SGS scalar variance production rate
r	separation between two points
S	skewness
$\mathbf{u}$	fluid velocity
$\langle \mathbf{u} \rangle_L$	resolvable-scale velocity
$\mathbf{v}$	sample-space variable for $\mathbf{u}$
VFJDF	velocity filtered joint density function
Z	mixture fraction
$\epsilon_{ij} = \nu \frac{\partial u_i}{\partial x_k} \frac{\partial u_j}{\partial x_k}$	velocity dissipation tensor
$\epsilon = \nu \frac{\partial u_i}{\partial x_k} \frac{\partial u_i}{\partial x_k}$	energy dissipation rate
$\epsilon_L = \langle \epsilon \rangle_L$	filtered energy dissipation rate
$\epsilon_r \ (= \epsilon_L)$	locally averaged energy dissipation rate
η	Kolmogorov length scale
$\chi = D \frac{\partial \phi}{\partial x_j} \frac{\partial \phi}{\partial x_j}$	scalar dissipation rate
$\chi_L = \langle \chi \rangle_L$	filtered scalar dissipation rate
$\chi_r \ (= \chi_L)$	locally averaged scalar dissipation rate
ν	kinematic viscosity
ξ	mixture fraction
$\langle \phi''^2 \rangle_L$	SGS scalar variance
$\langle \phi''^2 \rangle_r \ (= \langle \phi''^2 \rangle_L)$	local SGS scalar variance

III Findings

The velocity-scalar FJDF method was recently established by Peyman Givi and Stephen Pope [3]. It solves the velocity-scalar FJDF transport equation in which the SGS scalar transport term is in closed form. More importantly, this approach allows mixing models to depend on velocity, thus having the potential to provide a more realistic description of the SGS mixing, which is local in physical, velocity, and scalar spaces. Consistency with these conditions of localness is key to the accuracy of PDF-based approaches. We studied the FJDF and its transport equation for improving the velocity-scalar FJDF method.

The FJDF of velocity, $\mathbf{u}$, and scalar, ϕ is defined as

$$f_{u\phi}(\mathbf{v},\hat{\phi};\mathbf{x},t) = \int \prod_{i=1}^{3} \delta[u_i(\mathbf{x}',t) - v_i]\delta[\phi(\mathbf{x}',t) - \hat{\phi}]G(\mathbf{x}'-\mathbf{x})d\mathbf{x}', \tag{1}$$

where t, $\mathbf{x}$, $\mathbf{v}$, $\hat{\phi}$, δ, and G are time, the physical-space coordinates, the sample-space variables for $\mathbf{u}$ and ϕ, the Dirac delta function, and the filter function, respectively. The integration is over all physical space. The FJDF represents the weighted joint distribution of the velocity components and the scalar in a grid cell. The transport equation of the FJDF is obtained using the Navier-Stokes equations and the scalar transport equation:

$$\frac{\partial f_{u\phi L}}{\partial t} + v_j\frac{\partial f_{u\phi L}}{\partial x_j} = \frac{\partial \langle p\rangle_L}{\partial x_j}\frac{\partial f_{u\phi L}}{\partial v_j} + \frac{\partial}{\partial v_j}\{\langle \frac{\partial p'}{\partial x_j}|\mathbf{u}=\mathbf{v},\phi=\hat{\phi}\rangle_L f_{u\phi L}\}$$
$$-\frac{\partial}{\partial v_i}\{\langle \nu\frac{\partial^2 u_i}{\partial x_j\partial x_j}|\mathbf{u}=\mathbf{v},\phi=\hat{\phi}\rangle_L f_{u\phi L}\} - \frac{\partial}{\partial \hat{\phi}}\{\langle D\frac{\partial^2\phi}{\partial x_j\partial x_j}|\mathbf{u}=\mathbf{v},\phi=\hat{\phi}\rangle_L f_{u\phi L}\}. \tag{2}$$

where $\langle\cdot|\mathbf{u}=\mathbf{v},\phi=\hat{\phi}\rangle_L$ denotes a conditionally filtered variable conditional on the velocity vector and the scalar. The left hand side represents the time rate of change of the FJDF and transport of FJDF in physical space. The terms on the right hand side are transport of the FJDF in velocity space by the resolvable-scale pressure gradient, SGS pressure gradient, viscous acceleration, and molecular diffusion. An alternative term to the conditionally filtered scalar diffusion is the conditionally filtered scalar dissipation $\langle\chi|\mathbf{u}=\mathbf{v},\phi=\hat{\phi}\rangle_L$, where $\chi = D\frac{\partial\phi}{\partial x_j}\frac{\partial\phi}{\partial x_j}$ is the scalar dissipation rate.

Unlike a PDF, which is a statistic, the FJDF is a random process, and therefore requires statistical descriptions. In this research we employed conditional sampling and averaging techniques. Our previous studies of conserved scalar FDF and the FDF transport equation using these techniques [4, 5, 6] have shown that the SGS scalar has close-to-Gaussian and bimodal FDFs for small and large *instantaneous* SGS variance, respectively. In addition the SGS scalar is in spectral equilibrium (production of SGS variance smaller than dissipation) and non-equilibrium (production larger than dissipation), respectively. The bimodal SGS scalar contains diffusion layers, thus is similar to a nonpremixed scalar field. The results suggest that mixing models that can better predict the

non-equilibrium regime are needed. In this work we investigated the statistical dependence between the SGS velocity and scalar fields, and the effects of the SGS velocity on SGS scalar mixing. The FJDF and the SGS terms in the FJDF transport equation are analyzed using their conditional means with the SGS scalar variance $\langle \phi''^2 \rangle_L$ and the SGS kinetic energy, $k_L = (\langle u_1''^2 \rangle_L + \langle u_2''^2 \rangle_L)/2$ as conditioning variables.

We conducted experiments in an axisymmetric turbulent jet and used the experimental data to analyze the unclosed terms in the velocity-scalar FJDF and its transport equation. Measurements were made at 80 jet nozzle diameters, D, (=15 mm) downstream. The jet Reynolds number UD/ν was 40000. A sensor array consisting of three hot-wire probes was used to obtain data for performing filtering operations in both the streamwise (x) and transverse (y) directions. The filter size was varied from 63 to 250 Kolmogorov scales. This technique enabled us to acquire a large amount of data (2×10^8 samples) necessary to achieve sufficient statistical convergence.

In the following we briefly outline the results from our study and their implications for LES.

A. Galilean invariance of velocity PDF and FJDF

In turbulence and turbulent combustion modeling it is generally necessary for the model equations to have the same Galilean transformation properties as the exact transport equations. The Navier-Stoke equations and the moment equations for turbulent fluctuations are known to be Galilean invariant. Thus the modeled equations must also be Galilean invariant.

PDF methods have become an important modeling approach in turbulent flows, especially for reacting flows[7, 1]. In this approach the PDF transport equations are modeled. Although the modeled velocity PDF equations are implicitly assumed to be Galilean invariant in the literature[8], the Galilean transformation properties of both the exact and modeled PDF equations have not been given previously (even the transformation property of the PDF itself has not been discussed).

Another motivation for this analysis was the Galilean transformation properties of statistics conditional on turbulent velocity, which are important in studying turbulent flows. In fact, the key terms in the one-point PDF equation are means conditional on velocity at a point. Statistics conditional on the resolvable-scale velocity are also frequently used in analyses of the subgrid-scale stress and models in large eddy simulation. However, the Galilean invariance issue associated with such conditional statistics has not been previously addressed and there seems to be some confusion in the literature as to whether or not they are invariant under Galilean transformations. In this work we also considered this issue.

We first examined the transformation properties of the velocity joint probability density function

(JPDF)

$$f_u(\mathbf{v};\mathbf{x},t) = \langle \prod_{i=1}^{3} \delta[u_i - v_i] \rangle \tag{3}$$

where an $\langle\cdot\rangle$ denotes an ensemble mean. The Galilean transformations from one inertial reference frame $(\mathbf{x},t)$ to another $(\mathbf{x}^*,t^*)$ are

$$\mathbf{x}^* = \mathbf{x} + \mathbf{U}t, \quad t^* = t \tag{4}$$

where $\mathbf{U}$ is the (constant) velocity of the reference frame $(\mathbf{x},t)$ relative to $(\mathbf{x}^*,t^*)$. Thus a velocity field transforms as

$$\mathbf{u}^*(\mathbf{x}^*,t^*) = \mathbf{u}^*(\mathbf{x}+\mathbf{U}t,t) = \mathbf{u}(\mathbf{x},t) + \mathbf{U} \tag{5}$$

Thus the velocity is not invariant under Galilean transformations.

To transform the JPDF, in addition to the transformations in Eqs. 4 and 5, a transformation of the sample space is needed because the JPDF is also a function of $\mathbf{v}$. Since an event $\mathbf{u} = \mathbf{v}$ is equivalent to $\mathbf{u}^* = \mathbf{v} + \mathbf{U}$ in the new frame, the transformation is

$$\mathbf{v}^* = \mathbf{v} + \mathbf{U}. \tag{6}$$

Thus the sample space is not invariant. The transformation of the JPDF then is

$$f_u(\mathbf{v};\mathbf{x},t) = \langle \prod_{i=1}^{3} \delta[u_i - v_i] \rangle = \langle \prod_{i=1}^{3} \delta[u_i^* - U_i - (v_i^* - U_i)] \rangle = \langle \prod_{i=1}^{3} \delta[u_i^* - v_i^*] \rangle = f_{u^*}(\mathbf{v}^*;\mathbf{x}^*,t^*). \tag{7}$$

Therefore, the JPDF (as well as the fine-grained JPDF $\prod_{i=1}^{3} \delta[u_i - v_i]$) is invariant under Galilean transformations even though the velocity is not. The invariance of the JPDF is due to the invariance of $u_i - v_i$ in which the non-invariance of u_i and v_i is canceled. Since the transformations of both the velocity and the sample space are involved, the transformation of the JPDF is conceptually somewhat different from those we usually consider, such as the Reynolds stress and subgrid-scale stress. An intuitive way to understand the invariance of the JPDF is that one obtains the same JPDF values using the variables before and after the transformations. Equation 7 shows that the functional form of f_{u^*} is the same as f_u shifted by the amounts $\mathbf{U}$ and $\mathbf{U}t$ in the velocity sample space and in physical space, respectively.

Because the sample-space variable is an independent variable, the transformation is in a way similar to that for a scalar variable ϕ. We note that the transformation of the sample space is a key step in establishing the Galilean transformation property of the JPDF. If this step is omitted, the transformation group is incomplete, and a transformation $\mathbf{v}^* = \mathbf{v}$ is implied. The incomplete group results in the transformation $f_u(\mathbf{v};\mathbf{x},t) = f_{u^*}(\mathbf{v}^* + \mathbf{U};\mathbf{x}^*,t^*)$. Thus the JPDF appears as

non-invariant. The transformations in Eqs. 6 and 7 preserve the transformation properties of the moments of the JPDF (for example, the Reynolds stress $\langle u_i' u_j' \rangle = \langle u_i^{*\prime} u_j^{*\prime} \rangle$).

The JPDF transport equation is obtained from the Navier-Stokes equations and the definition Eq. 3[7]

$$\frac{\partial f_u}{\partial t} + v_j \frac{\partial f_u}{\partial x_j} = \frac{\partial}{\partial v_i}\{\langle \frac{\partial p}{\partial x_i} | \mathbf{u} = \mathbf{v} \rangle f_u\} - \frac{\partial}{\partial v_i}\{\langle \frac{\partial^2 u_i}{\partial x_j \partial x_j} | \mathbf{u} = \mathbf{v} \rangle f_u\}, \tag{8}$$

where $\langle \cdot | \mathbf{u} = \mathbf{v} \rangle$ is a mean conditional on the velocity. Using the transformations in Eqs. 2, 3, 8 and 9, the transformations of the terms in the JPDF equation can be obtained as follows:

$$\frac{\partial f_u}{\partial t} = \frac{\partial f_{u^*}}{\partial t^*} + \frac{\partial f_{u^*}}{\partial x_j^*}\frac{\partial x_j^*}{\partial t} = \frac{\partial f_{u^*}}{\partial t^*} + U_j \frac{\partial f_{u^*}}{\partial x_j^*}, \quad \frac{\partial f_u}{\partial x_j} = \frac{\partial f_{u^*}}{\partial x_j^*}, \tag{9}$$

$$\frac{\partial}{\partial v_i}\{\langle \frac{\partial p}{\partial x_i} | \mathbf{u} = \mathbf{v} \rangle f_u\} = \frac{\partial}{\partial v_i^*}\{\langle \frac{\partial p^*}{\partial x_i^*} | \mathbf{u}^* = \mathbf{v}^* \rangle f_{u^*}\} \tag{10}$$

$$\frac{\partial}{\partial v_i}\{\langle \frac{\partial^2 u_i}{\partial x_j \partial x_j} | \mathbf{u} = \mathbf{v} \rangle f_u\} = \frac{\partial}{\partial v_i^*}\{\langle \frac{\partial^2 u_i^*}{\partial x_j^* \partial x_j^*} | \mathbf{u}^* = \mathbf{v}^* \rangle f_{u^*}\}. \tag{11}$$

Therefore the JPDF transport equation is invariant under Galilean transformations. The invariance might not seem intuitive since the conditional averages in Eqs. 10 and 11 shift in the velocity sample-space under Galilean transformations. However, because $\mathbf{v}$ is an independent variable, dependence on it is generally expected and does not lead to non-invariance as long as the forms of the transformed terms are invariant. Thus both the JPDF equation and its solutions (as well as the initial/boundary conditions) are Galilean invariant, In contrast, while the Navier-Stokes equations are Galilean invariant, their solutions are not.

The conditional means in Eqs. 10 and 11 are Galilean invariant because the conditioning event $\mathbf{u} = \mathbf{v}$ is equivalent to $\mathbf{u}^* = \mathbf{v} + \mathbf{U} = \mathbf{v}^*$ in the new reference frame. This argument also leads to Galilean invariance of the conditional statistics of any Galilean invariant variable conditional on the velocity. The invariant property provides an important basis for using conditional statistics conditional on the velocity in studying turbulent flows and for extending results to other inertial reference frames. Again, the key step leading to the invariance is the transformation of the sample space. Like the velocity JPDF, the conditional statistics appear as non-invariant if this transformation is omitted. This fact might be a cause for the confusion in the literature as to whether the conditional statistics are Galilean invariant or not.

The above analyses were extended to the filtered joint density function (FJDF) used in PDF-based large-eddy simulation and its transport equation[2]. Speziale[9] showed that the filtered (large-scale) part of a Galilean invariant function is also Galilean invariant. Because the fine-grained JPDF is Galilean invariant, its filtered part, the FJDF

$$\int \prod_{i=1}^{3} \delta[u_i(\mathbf{x}', t) - v_i] G(\mathbf{x}' - \mathbf{x}) d\mathbf{x}' = \int \prod_{i=1}^{3} \delta[u_i^*(\mathbf{x}^{*\prime}, t^*) - v_i^*] G(\mathbf{x}^{*\prime} - \mathbf{x}^*) d\mathbf{x}^{*\prime} \tag{12}$$

is also Galilean invariant. Thus all Galilean-invariant models for the PDF methods can be extended to PDF-based large-eddy simulation.

In summary, the JPDF and its transport equation were shown to be Galilean invariant. For constant density flows they are also invariant under extended Galilean transformations. In addition, the conditional means in the JPDF equation as well as the conditional statistics of any Galilean invariant variables conditional on the velocity are invariant. A key step in establishing these transformation properties is the proper transformation of the sample-space variable which makes the group of Galilean transformations complete. The present work provides support for PDF methods and a basis and justification for studying turbulent flows and turbulent combustion using statistics conditional on the velocity.

B. Velocity FJDF, conditionally filtered viscous acceleration, and dissipation

We now discuss the results on the velocity FJDF and its transport equation. The understanding gained provides a basis for studying the velocity-scalar FJDF.

Unlike a PDF, a VFJDF is not a statistic, but a random process and must be characterized statistically. For a filter size smaller than the integral length scale, the mean VFJDF approximately equals the velocity JPDF, which is generally not far from joint-Gaussian in regions of fully developed flows without large-scale intermittency[10, 11]. Therefore the mean VFJDF does not provide additional information on the VFJDF. However, other important characteristics of the VFJDF can be revealed by its conditional means. Recent results obtained by the PI on conditional scalar FDF and scalar-scalar-dissipation FJDF have provided important characteristics of the SGS scalar field[4, 5, 6]. The SGS scalar has been found to be in quasi-equilibrium (SGS production equal to or smaller than dissipation) and non-equilibrium (SGS production exceeds dissipation) for small and large SGS scalar variance, respectively[4, 5]. Here, for convenience, we refer to both the cases of SGS production equal to and smaller than dissipation as quasi-equilibrium because the SGS scalar has very similar characteristics for the two cases. The FDF and the terms in its transport equation in these two regimes have qualitatively different characteristics. For equilibrium SGS scalar fields the FDF is, on average, close to Gaussian (Fig. 1) and the scalar dissipation has only moderate dependence on the SGS scalar. These properties are similar to those of unfiltered scalar fluctuations in fully developed turbulent flows; however, for non-equilibrium SGS scalar fields (at large SGS scalar variance), the FDF is bimodal, and the scalar dissipation depends strongly on the SGS scalar. The SGS scalar is also characterized by the existence of diffusion-layer-like structure (ramp-cliffs). These characteristics are similar to the scalar PDF in the early stages of initially binary mixing[12]. Therefore, when used as a conditioning variable for the conditional scalar FDF, the SGS scalar variance can reveal the structure of the SGS scalar that is otherwise averaged out, providing important new SGS physics. This property of the SGS variance is partly because it is an

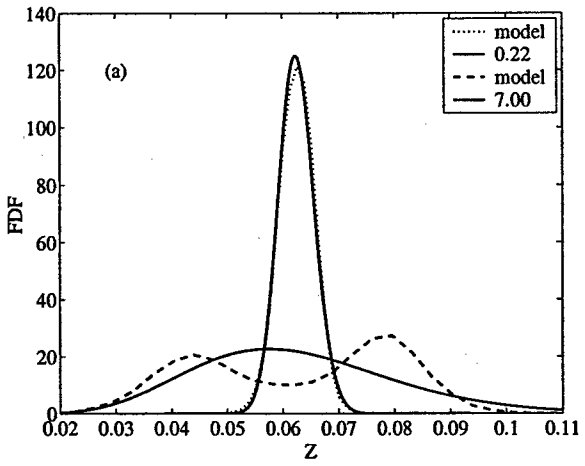

Figure 1: Conditional FDF of mixture fraction, Z, in the jet. The FDF is Gaussian and bimodal for small and large SGS variance values, respectively. The beta model is able to predict the Gaussian FDF but not the bimodal FDF. The SGS variance normalized by its mean is given in the legend.

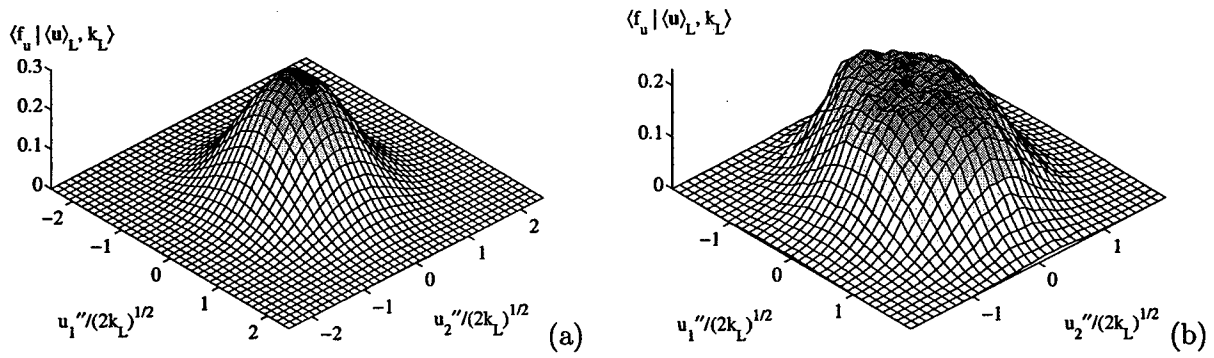

Figure 2: Mean FJDF conditional on the SGS energy and the resolvable-scale velocity: (a) $k'_L/\langle k_L\rangle = 0.33$, $\langle u_1\rangle_L = \langle u\rangle$ (3 m/s), $\langle u_2\rangle_L = 0$. The FJDF is close to joint-Gaussian; (b) $k_L/\langle k_L\rangle = 4.2$, $\langle u\rangle_L = \langle u\rangle$ (3 m/s), $\langle v\rangle_L = 0$. The FJDF has an approximately uniform region.

important variable in the inertial-range dynamics and for characterizing the state of SGS mixing. Since the conditional scalar FDF for different SGS variance is dominated by different structures and dynamics, it can potentially be modeled more accurately than the unconditioned FDF (or PDF), leading to improved LES statistics. Therefore, such conditional FDFs are important for studying SGS scalars and modeling SGS mixing.

The mean FJDF conditional on the SGS energy, k_L, and the resolvable-scale velocity, $\mathbf{u}_L$ is shown in Fig. 2. For small SGS energy the conditional FJDF is close to joint-Gaussian, similar to the JPDF in a fully developed turbulent jet, which is in quasi-equilibrium. For large SGS energy ($k_L/\langle k_L\rangle = 4.2$) the FJDF has an approximately uniform region, beyond which the FJDF decreases rapidly (faster than joint-Gaussian). The existence of the uniform region suggests that the SGS

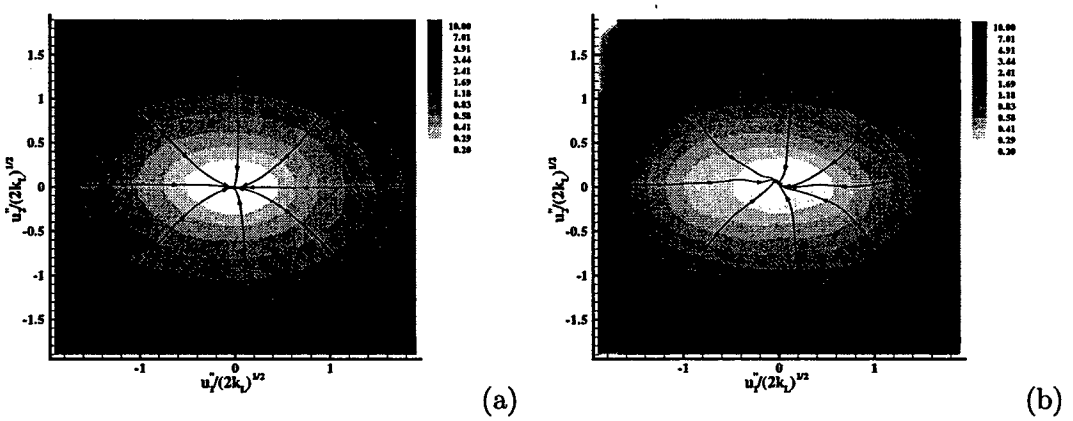

Figure 3: Streamline plots of the conditional filtered viscous acceleration for $\Delta/\eta = 125$, $\langle\langle\nu(\frac{\partial^2 u_1}{\partial x_1^2}, \frac{1}{2}\frac{\partial^2 u_2}{\partial x_1^2})|u_1, u_2\rangle_L|\langle\mathbf{u}\rangle_L, k_L\rangle\frac{(2k_L)^{1/2}}{\langle\epsilon_L|k_L\rangle}$. $\langle u_1\rangle_L = \langle u_1\rangle$ and $\langle u_2\rangle_L = 0$. (a) $k_L/\langle k_L\rangle = 1.2$, (b) $k_L/\langle k_L\rangle = 4.6$. The magnitudes of these variables are given as grayscales.

velocity field under this condition contains structures in which the velocity varies approximately linearly in physical space. Examples of such structures include axisymmetric contraction and expansion, plane strain, and plane strain plus plane shear. Since these local structures occur at large k_L, the strain rate imposed by them is larger than the average turbulent strain rate near the filter scale. As a result, the production of the SGS energy increases, and, when the strain rate is sufficiently large, the "background" SGS turbulence (the SGS turbulence minus the structure) may be undergoing local rapid distortion, suggesting that the SGS velocity field is in non-equilibrium, because rapid distortion is a linear process and spectral transfer is not effective in responding to the increased SGS energy production. Therefore, the dissipation lags behind the production, resulting in local non-equilibrium. Also see discussions in Part C.

Since wavenumber information is needed to describe turbulence under rapid distortion, a conventional one-point PDF model is not sufficient. To overcome this difficulty, Van Slooten and Pope (1997) developed a velocity-wave-vector PDF model that gives the exact Reynolds stress in the rapid distortion limit. The present study suggests that local rapid distortion might exist even when the mean strain rate is not large. Thus it may be beneficial to adopt this model for LES so that the local rapid distortion effects can be taken into account.

In the present study two (partial) components of the viscous acceleration were measured. The conditionally filtered viscous acceleration, $\langle\nu(\frac{\partial^2 u_1}{\partial x_1^2}, \frac{1}{2}\frac{\partial^2 u_2}{\partial x_1^2})|u_1, u_2\rangle_L$, conditional on the velocity components represents the transport velocity of the VFJDF by viscous acceleration in the velocity space and is shown in Fig. 3 as streamline plots. A factor of 1/2 was used for the u_2 component because for isotropic turbulence its rms is twice that of the u_1 component. The magnitude of the

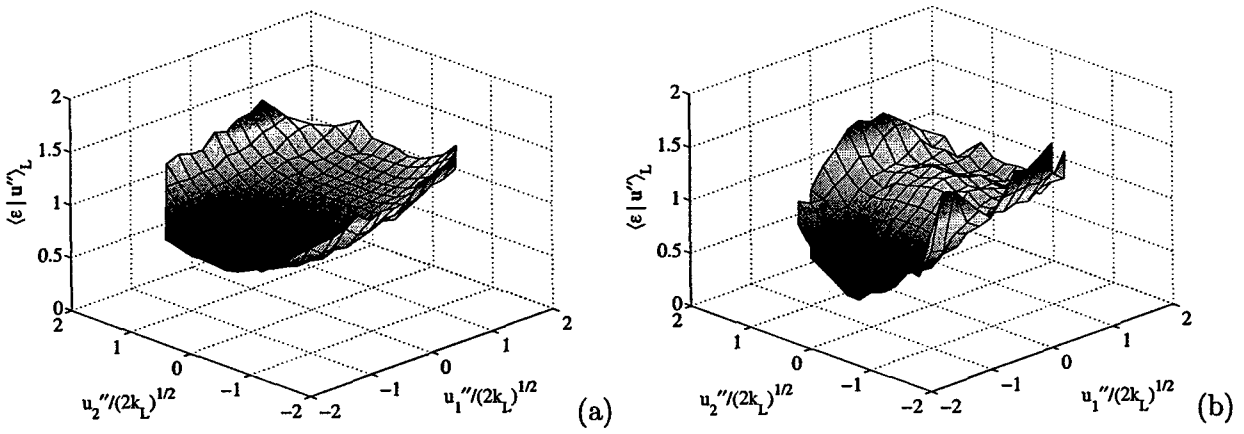

Figure 4: The conditionally filtered energy dissipation rate $\langle\langle\epsilon|u_1,u_2\rangle_L|\langle\mathbf{u}\rangle_L,k_L\rangle/\langle\epsilon_L|k_L\rangle$ The conditions are the same as in Fig. 3.

vector field, normalized by $(2k_L)^{1/2}/\langle\epsilon_L|k_L\rangle$, is given as gray scale isocontours. The streamlines generally flow towards a stagnation point, which is approximately at the center of the VFJDF. The magnitude of the acceleration increases with the magnitude of the velocity. This dependence is similar to that of the scalar diffusion on the value of the scalar[13, 14, 15]. The conditional viscous acceleration in the velocity JPDF equation, $\langle\nu(\frac{\partial^2 u_1}{\partial x_1^2},\frac{1}{2}\frac{\partial^2 u_2}{\partial x_1^2})|u_1,u_2\rangle$, also has similar properties [Fig. 11(c)]. The normalized magnitude of the conditionally filtered viscous acceleration increases faster for larger the SGS energy, probably because the local rapid distortion at large SGS energy causes the SGS fluctuations and accelerations to increase, although the linear portion of the SGS velocity does not directly contribute to viscous acceleration. The observed rate of increase might also be partially due to the decrease in the normalized sample-space variable $\mathbf{v}/(2k_L)^{1/2}$. We note that, although the conditional viscous acceleration is non-negligible, the rms viscous acceleration becomes smaller than the rms pressure gradient as Reynolds number increases[16].

The conditionally filtered dissipation tensor, $\langle\epsilon_{ij}|u_1,u_2\rangle_L$, provides an alternative to the conditionally filtered viscous acceleration to close the VFJDF equation, where $\epsilon_{ij}=\nu\frac{\partial u_i}{\partial x_k}\frac{\partial u_j}{\partial x_k}$. Figure 4 shows the surface plots for the conditionally filtered energy dissipation rate $\langle\epsilon|u_1,u_2\rangle_L$ normalized by the filtered energy dissipation rate, $\langle\epsilon_L|k_L\rangle$. In general, the dissipation increases with u_1. For small SGS energy the surface is concave, similar to the dependence of the scalar dissipation on the scalar values for small SGS variance. The surface plot for the conditional energy dissipation $\langle\epsilon|u_1,u_2\rangle$, which appears in the velocity JPDF equation, also has a similar shape. For large SGS energy there is a slight bulge in the center portion of the surface, suggesting that the local velocity field responsible for the large strain rate deviates somewhat from a linear field because the dissipation is constant in such a field. Nonetheless, the deviation is small, as indicated by the uniform portion of the conditional VFJDF. The moderate dependence of the dissipation on the SGS velocity

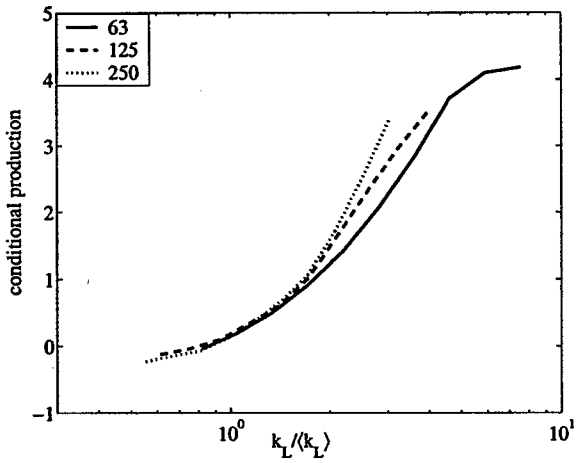

Figure 5: Conditional production of SGS energy (energy transfer rate) normalized by the filtered energy dissipation rate, $\langle(\langle u_i u_j\rangle_L - \langle u_i\rangle_L\langle u_j\rangle_L)s_{ij}|k_L\rangle/\langle\epsilon_L|k_L\rangle$. The production exceeds the dissipation for large values of k_L, indicating non-equilibrium SGS velocity. The filter sizes are given in the legend.

suggests that the current practice of modeling the dissipation independent of the velocity is largely justified.

C. Structure of the SGS velocity

The non-universal VFJDF raises questions about the structure of the SGS velocity field. We investigated the structure, which is important for modeling VFJDF. In turbulence under rapid distortion, the spectral energy transfer rate is small compared to the production due to the mean strain. Thus, the turbulent fluctuations gain more energy than the spectral transfer (and than the dissipation) can remove, suggesting non-equilibrium turbulence. The SGS turbulence under rapid distortion is also found to be in non-equilibrium[17]. To determine whether the SGS turbulence under *local* rapid distortion is in non-equilibrium, we compared the production rate of the SGS energy, $\tau_{ij}s_{ij}$, to the filtered dissipation rate ϵ_L. Here τ_{ij} is defined as $\langle u_i u_j\rangle_L - \langle u_i\rangle_L\langle u_j\rangle_L$. We used $\frac{15}{6}(\tau_{11}s_{11}+2\tau_{12}s_{12}+\tau_{22}s_{22})$ and $5\nu[(\frac{\partial u_1}{\partial x_1})^2+(\frac{\partial u_2}{\partial x_1})^2]$ as surrogates for the full energy production rate and the full dissipation rate, respectively. Figure 5 gives the ratio of the conditional production of the SGS energy to the conditional dissipation conditional on the SGS energy. Indeed, the conditional production exceeds the conditional dissipation when the SGS energy is larger than its mean value, indicating that the spectral transfer is not effective in responding to the increased SGS energy production and that the SGS turbulence is in non-equilibrium. This result is consistent with those for SGS turbulence under rapid distortion by the mean flow[17]. The non-equilibrium of the SGS velocity is similar to the non-equilibrium of the SGS scalar when the SGS variance is large[5]. Like the non-equilibrium SGS scalar, which contains scalar structures (diffusion layers), the non-equilibrium SGS velocity also contains structures.

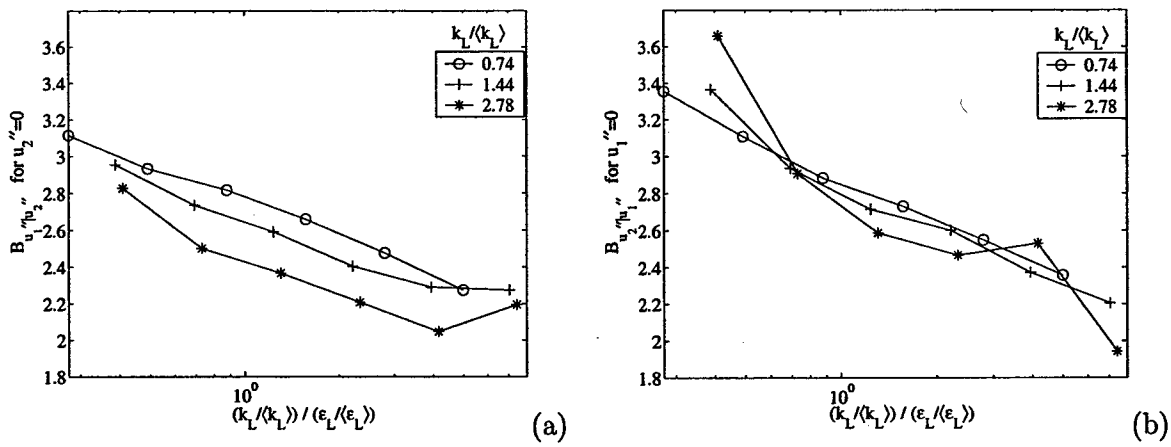

Figure 6: The parameters B as a function of k_L/ϵ_L for $\Delta/\eta = 125$ for different k_L values. The collapse of the curves indicates that the VFJDF can largely be characterized by $k_L/\epsilon_L/(\langle k_L\rangle/\langle\epsilon_L\rangle)$.

To further examine the effects of the non-equilibrium SGS turbulence on the VFJDF we computed the conditional VFJDF with the filtered dissipation ϵ_L used as an additional conditioning variable. The SGS dissipation time scale, k_L/ϵ_L, can be used as an indicator of the degree of the non-equilibrium: large SGS time scale indicates that dissipation is not fast enough, and the SGS turbulence is in non-equilibrium.

To quantify the dependence of the shape of the VFJDF on k_L and ϵ_L, we used two slices of the VFJDF going through the origin in the v_1 and v_2 directions, respectively. We computed the conditional kurtosis and skewness of the VFJDF, $K_{u_1|u_2}$ and $S_{u_1|u_2}$ (for $u_2 = 0$), which can be obtained from the conditional fourth and third moments of $\langle f_{u_1|u_2}(v_1)|k_L, \epsilon_L, \langle \mathbf{u}\rangle_L\rangle$, normalized by the second moment raised to the proper power, where $f_{u_1|u_2}$ is the FDF of the u_1 component conditional on the u_2 component (essentially a slice in the u_1 direction). The conditional kurtosis and skewness $K_{u_2|u_1}$ and $S_{u_2|u_1}$ can also be obtained in the same way. We combined K and S to form a parameter $B = K - S^2$, proposed by Atkinson[18]. This parameter takes the value of unity for a double-delta PDF regardless of its symmetry, therefore, is a better measure of the intermittency (or lack of) than the kurtosis. For a uniform distribution B has a value of 1.8. It has been used to characterize the bimodal scalar FDF[4] and velocity increment PDF[19].

We examined $B_{u_1|u_2}$ for $u_2'' = 0$ and $B_{u_2|u_1}$ for $u_1'' = 0$. If the VFJDF is perfectly uniform both parameters have the value of 1.8. Figure 6 shows that B generally decreases with ϵ_L, consistent with the observation that the VFJDF changes towards a uniform shape as ϵ_L decreases. Due to the opposite trends of B with respect to k_L and ϵ_L, we plotted $B_{u_1|u_2}$ and $B_{u_2|u_1}$ against k_L/ϵ_L for three k_L values. Figure 6 shows that both $B_{u_1|u_2}$ and $B_{u_2|u_1}$ decrease as k_L/ϵ_L increases. Furthermore, the curves for $B_{u_2|u_1}$ appear to collapse for different k_L values, although the results for $B_{u_1|u_2}$ still show some k_L dependence. Nonetheless, these results indicate that k_L/ϵ_L alone

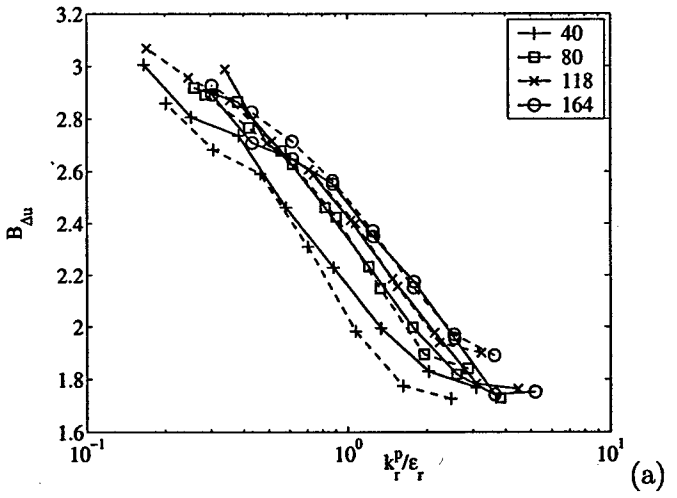

Figure 7: Dependence of the bimodality parameter on k_r^p/ϵ_r. The averaging domain sizes are given in the legend. The values of p is approximately 0.76. The the dashed and solid lines represent $k_r/\langle k_r \rangle$ values of 1.0 and 4.0 respectively. Except for $r/\eta = 40$, $B_{\Delta u}$ is essentially determined by k_r^p/ϵ_r and is independent of k_r.

can largely characterize the shape of the VFJDF. Specifically, the VFJDF is uniform as long as k_L/ϵ_L is large, i.e., when the SGS velocity is in strong non-equilibrium, regardless of the value of k_L. This condition is less restrictive than that of $k_L/\langle k_L \rangle \gg 1$. The observed importance of k_L/ϵ_L in determining $B_{u_1|u_2}$ and $B_{u_2|u_1}$ suggests that the degree of non-equilibrium is important for determining the distribution of the SGS velocity field.

To further understand the structure of the SGS velocity, we also examined the conditional velocity increment with separations the same as the filter sizes. The increment explicitly contains (two-point) spatial information whereas the VFJDF only contains information implicitly. Therefore, conditional velocity increment statistics provide essential information complementing the VFJDF.

In Fig. 7 we plotted the bimodality parameter conditional on k_L and ϵ_L (here k_r and ϵ_r are used for k_L and ϵ_L to indicate that the results are for increments) and for the velocity increment PDF as a function of k_L^p/ϵ_L, where p is the scaling exponent for $\langle \epsilon_r | k_r \rangle \sim k_r^p$. We choose the ratio of $\langle \epsilon_r | k_r \rangle / \epsilon_r \sim k_r^p/\epsilon_r$ as the variable because it is an indicator of the deviation of ϵ_r from its conditional mean. For a randomly oriented plane strain field, $B_{\Delta u}$ is bimodal. For all separations considered, $B_{\Delta u}$ decreases with k_r^p/ϵ_r, and the increment PDF is bimodal for large k_r^p/ϵ_r values. Furthermore, $B_{\Delta u}$ is approximately independent of the k_r values, indicating that the bimodality is largely determined by the relative magnitude of ϵ_r to its conditional mean, suggesting that the

bimodality is closely related to the degree of non-equilibrium of the local velocity field because as k_r^p/ϵ_r increases the production of k_r increases relative to the dissipation. The bimodality parameter $B_{\Delta v}$ has a similar trend, but there is still some weak dependence on k_r. Furthermore, it appears that the curves for different filter scales can be collapsed by shifting them horizontally, i.e., by a multiplying factor to k_r^p/ϵ_r. Except for $r/\eta = 40$, this factor ranges from 1.1 to 1.5. Thus, the need for this factor might be a result of the limited Reynolds number (and the scale separations between r and the integral length scales) in the present study. At higher Reynolds numbers, we might expect improved scaling regions for $k_r^{-p}\langle\epsilon_r|k_r\rangle$ and collapse of the results for the bimodality parameter. This result suggests that there may be "universal" dependence of the bimodality on k_r^p/ϵ_r. Thus, the results provide further evidence of the plane strain structure inferred from the VFJDF.

D. Velocity-scalar FJDF, conditionally filtered scalar diffusion, and dissipation

This part focuses on the coupling between the SGS velocity and scalars, which is essential for modeling the effects of the velocity on the SGS mixing.

The mean FJDF conditional on four variables: the SGS energy, the resolvable-scale velocity, the SGS scalar variance, and the resolvable-scale scalar has qualitatively different forms depending on the conditioning variables. For small k_L ($< \langle k_L \rangle$) and $\langle\phi''^2\rangle_L$ ($< \langle\phi''^2\rangle$), the conditional FJDF is close to joint-Gaussian (not shown), similar to the JPDF in a fully developed turbulent jet, which is generally in quasi-equilibrium. For large $\langle\phi''^2\rangle_L$ the FJDF is bimodal at $\phi''/\langle\phi''^2\rangle_L \approx \pm 1$ regardless of the values of k_L (Fig. 8), consistent with a scalar diffusion layer structure. For small k_L [Fig. 8(a)] the correlation between the SGS scalar and the velocity component u_1 is low, indicating small conditional SGS flux. For large k_L [Fig. 8(b)] the correlation is strong, and the two peaks of the FJDF are also separated in the velocity space with a "neck" near $u_1 = 0$. Thus, scalar mixing is expected to be most intense near this point and depends strongly on the velocity, further demonstrating the need for mixing models to depend on the velocity. This FJDF shape is consistent with a scalar diffusion layer associated with a local plane strain (converging-diverging) velocity field. In such a structure the scalar gradient is largest in the diffusion layer, where the SGS velocity is the smallest. The structure is similar to the counter-flow model for laminar flamelets. The FJDF peaks in Fig. 8(a), on the other hand, overlap in the velocity space. Thus mixing can occur over a wide range of SGS velocity and is less dependent on the velocity.

In the present study the scalar diffusion and dissipation were obtained using the streamwise derivatives. For small $\langle\phi''^2\rangle_L$ the diffusion generally has linear dependence on both the SGS velocity and scalar. Figure 9(a) shows the conditionally filtered diffusion for small k_L ($0.52\langle k_L \rangle$). In the center portion the isocontours can be approximated by equally-spaced straight lines, consistent with a previous linear model. For large k_L the isocontours have a larger slope, indicating a stronger

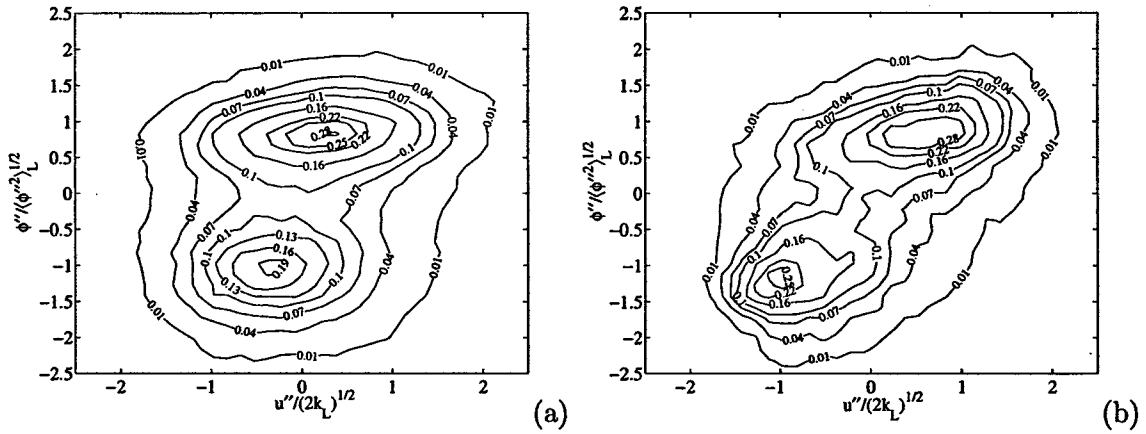

Figure 8: Mean FJDF conditional on k_L, $\langle \mathbf{u} \rangle_L$, $\langle \phi''^2 \rangle_L$, and $\langle \phi \rangle_L$ on the jet centerline for $\langle u_1 \rangle_L = \langle u_1 \rangle$ (3.07 m/s) and $\langle u_1 \rangle_L = 0$: (a) $k_L/\langle k_L \rangle = 3.04$ and $\langle \phi''^2 \rangle_L/\langle \phi''^2 \rangle = 6.09$; (b) $k_L/\langle k_L \rangle = 0.64$ and $\langle \phi''^2 \rangle_L/\langle \phi''^2 \rangle = 6.09$. The bimodal FJDF in (b) is strongly asymmetric in u_1, indicating large SGS flux and suggesting that mixing occurs primarily near $u_1 = 0$.

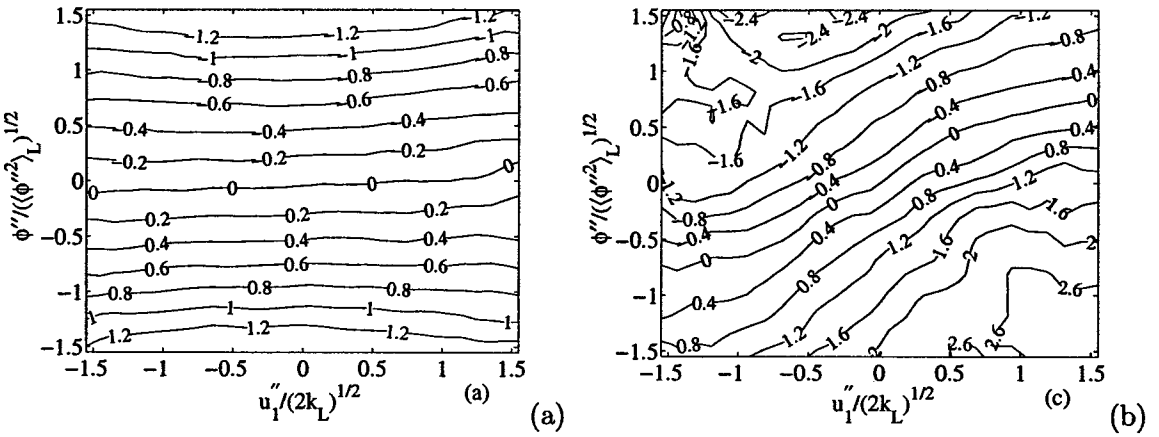

Figure 9: Mean conditionally filtered scalar diffusion: (a) $k_L/\langle k_L \rangle = 0.8$ and $\langle \phi''^2 \rangle_L/\langle \phi''^2 \rangle = 0.94$; (b) $k_L/\langle k_L \rangle = 0.52$ and $\langle \phi''^2 \rangle_L/\langle \phi''^2 \rangle = 6.09$. The diffusion in (a) is can be approximated using a previous linear model (straight lines) whereas that in (b) has a S-shaped region.

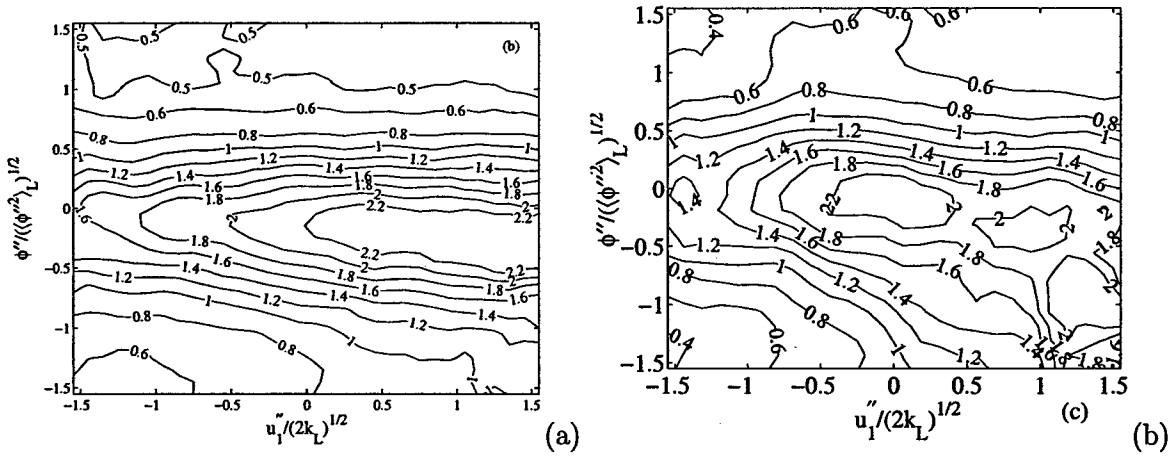

Figure 10: Normalized mean conditionally filtered scalar dissipation: (a) $k_L/\langle k_L\rangle = 0.64$ and $\langle\phi''^2\rangle_L/\langle\phi''^2\rangle = 4.67$; (b) $k_L/\langle k_L\rangle = 2.43$ and $\langle\phi''^2\rangle_L/\langle\phi''^2\rangle = 4.67$. The dissipation in (b) shows that mixing occurs primarily near $u_1 = 0$.

dependence on u_1. The results are consistent with velocity-scalar fields having a joint normal JPDF.

For large SGS variance the surface plot of the diffusion is S-shaped and depends on u_1 for certain ranges of k_L values. Figure 9(b) shows the conditionally filtered diffusion for large $\langle\phi''^2\rangle_L$ ($6.09\langle\phi''^2\rangle$) but small k_L. In addition to an approximately linear trend, an S-shaped dependence on ϕ exists for all u_1 values, consistent with the FJDF in Fig. 8(a), which shows that the bimodal scalar distribution spans a wide range of velocity. For large k_L the S-shaped region appears to be limited to near $u_1 = 0$ (not shown), suggesting that large magnitudes of diffusion occur at small SGS velocity. This issue is further discussed in the following, along with the dissipation.

The conditionally filtered scalar dissipation provides an alternative to the conditionally filtered scalar diffusion to close the FJDF equation. For small $\langle\phi''^2\rangle_L$ the dissipation generally depends weakly on both the velocity and scalar (not shown), consistent with the approximately joint normal FJDF. For small k_L and large $\langle\phi''^2\rangle_L$ the dissipation shown in Fig. 10(a) has a bell-shaped dependence on ϕ but is weakly dependent on u_1. The dependence on ϕ is consistent with the FJDF in Fig. 8(a) and the S-shaped diffusion plot in Fig. 9(b). For large k_L and $\langle\phi''^2\rangle_L$ the dissipation is largest at $\phi = 0$ and $u_1 = 0$ [Fig. 10(b)] and decreases as velocity increases, indicating a strong dependence on the SGS velocity, consistent with the FJDF in Fig. 8(b) and the notion that the diffusion layer is associated with a converging-diverging (e.g., plane strain) velocity field. In such a structure the velocity component normal to the diffusion layer is small near the layer. This result also suggests that the S-shaped surface for the scalar diffusion is limited to small u_1 values. Since diffusion layers have been shown to exist at very high Reynolds numbers, the observed dependence of scalar diffusion and dissipation on the velocity is expected to be Reynolds-number independent.

This study showed that there is a strong statistical dependence between scalar mixing (dissipation-

scale scalar) and the SGS velocity field. The scalar and velocity structure for large SGS variance (especially when the SGS energy is also large) is similar to the structure of laminar flamelets. Thus the ability of mixing model to reflect such a structure and the localness of mixing is important. The scalar diffusion conditional on the SGS velocity under such conditions is expected to be non-zero and independent of Reynolds number. The results further demonstrate the importance of the velocity in mixing and of including velocity in mixing models.

E. The joint structure of SGS velocity and scalar

The velocity-scalar FJDF observed suggests coupled structures of the SGS velocity and scalars. We investigated the velocity-scalar increment JPDFs to further examine the structures.

When conditioned on ϵ_r and χ_r (again, r is used in the subscript instead of a L to indicate that the results are for increments), the joint PDF of velocity and scalar increments, $P_{\Delta v,\Delta\phi|\epsilon_r,\chi_r}$ is close to joint Gaussian for a range of ϵ_r and χ_r values, consistent with Kolmogorov's refined similarity hypotheses (K62)[20]. When conditioned on the local kinetic energy and the local scalar variance, $P_{\Delta v,\Delta\phi|k_r,\langle\phi''^2\rangle_r}$ has different shapes depending on the values of the conditioning variables. For small $\langle\phi''^2\rangle_r$ and k_r, it is close to joint normal [Fig. 11 (a)]. For small $\langle\phi''^2\rangle_r$ but large k_r, it is bimodal in Δv, indicating a well-mixed local scalar field but a nonequilibrium local velocity field. The results in Part C.[21] have shown that when k_r is large the local turbulence is under rapid distortion, and the local velocity field contains plain strain. Figure 11 (b) suggests that the plane strain does not alter the distribution of a well-mixed scalar. For large $\langle\phi''^2\rangle_r$ but small k_r, $P_{\Delta v,\Delta\phi|k_r,\langle\phi''^2\rangle_r}$ is bimodal in $\Delta\phi$, indicating a nonequilibrium local scalar field but an equilibrium local velocity field. Although the velocity is in quasi-equilibrium at scale r, the bimodal JPDF suggests that there may be nonequilibrium velocity fields at smaller scales. Therefore, the diffusion layers under such conditions might be highly wrinkled. When both $\langle\phi''^2\rangle_r$ and k_r are large, $P_{\Delta v,\Delta\phi|k_r,\langle\phi''^2\rangle_r}$ is quad-modal, with one peak in each quadrant of the $\Delta v - \Delta\phi$ plane. This JPDF shape has not been previously observed for inertial-range turbulence and provides further evidence of the combination of a local plane strain and ramp-cliff (diffusion layer) structure.

The similarity between the SGS scalar at large SGS variance and binary mixing suggests that the SGS scalar is in nonequilibrium. To further examine the role played by spectral nonequilibrium, we computed the conditional production rate of $\langle\phi''^2\rangle_r$, $\mathcal{P}_{\phi r} = -(\langle u_j\phi\rangle_r - \langle u_j\rangle_r\langle\phi\rangle_r)\dfrac{\partial\langle\phi\rangle_r}{\partial x_j}$, conditional on $\langle\phi''^2\rangle_r$ and χ_r, respectively (Fig. 12). The averaging domain size r is 125η. When conditioned on $\langle\phi''^2\rangle_r$, the conditional mean of $\mathcal{P}_{\phi r}$ normalized by $\langle\chi_r|\langle\phi''^2\rangle_r\rangle$ is small for $\langle\phi''^2\rangle_r/\langle\phi''^2\rangle < 1$ and increases with $\langle\phi''^2\rangle_r$ ($\sim \langle\phi''^2\rangle_r^{0.8}$), indicating that the local scalar field changes from quasi-equilibrium to nonequilibrium as $\langle\phi''^2\rangle_r$ increases. (A decaying scalar field has similar characteristics to a quasi-equilibrium scalar field). On the other hand, when conditioned on the scalar dissipation, $\mathcal{P}_{\phi r}/\chi_r$ only increases by a factor of two over two orders of magnitude increase in χ_r. The results

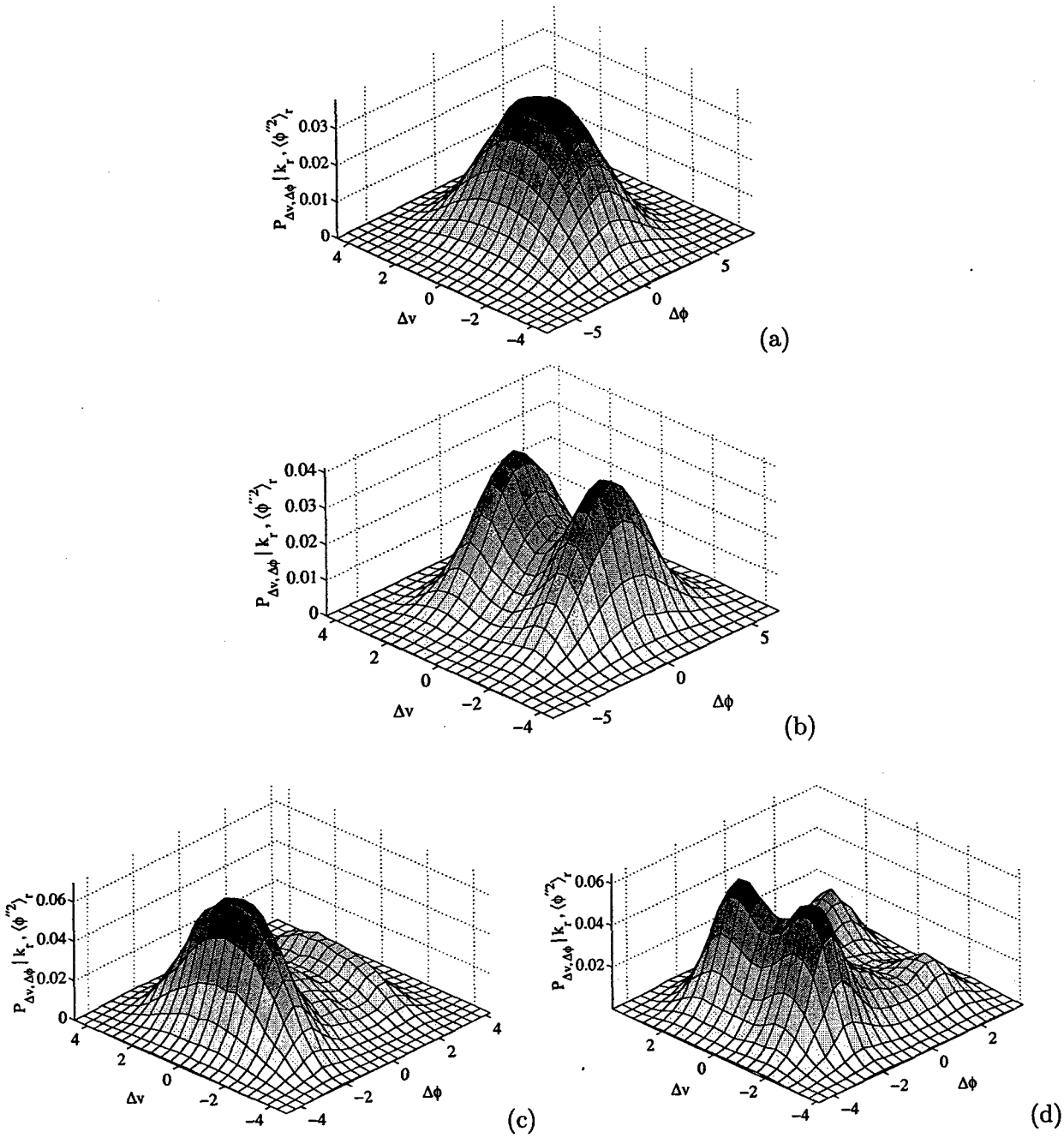

Figure 11: Conditional JPDF of Δv and $\Delta\phi$ conditional on k_r and $\langle\phi''^2\rangle_r$. The values of $k_r/\langle k_r\rangle$ and $\langle\phi''^2\rangle_r/\langle\phi''^2\rangle$ are (a) 0.06, 0.3; (b) 6.0, 0.3; (c) 0.06, 8.0; (d) 6.0, 8.0.

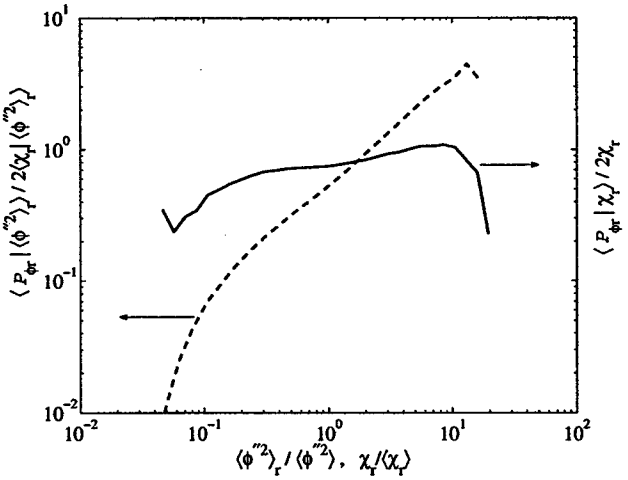

Figure 12: Conditional mean of the local scalar variance production $\mathcal{P}_{\phi r}$, conditional on $\langle \phi''^2 \rangle_r$ and χ_r, respectively. The averaging domain size r is 125η.

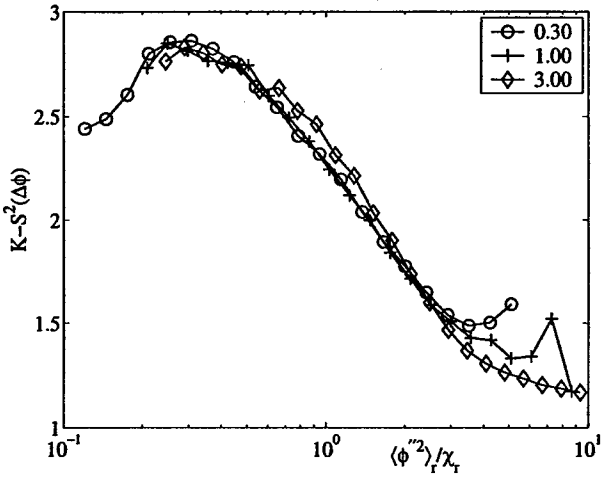

Figure 13: Dependence of the bimodality parameter on $\langle \phi''^2 \rangle_r / \chi_r$. The values of $\langle \phi''^2 \rangle_r / \langle \phi''^2 \rangle$ are given in the legend. B is essentially determined by $\langle \phi''^2 \rangle_r / \chi_r$, independent of $\langle \phi''^2 \rangle_r$.

suggest that when conditioned on χ_r, the conditional inertial-range scalar is, on average, in quasi-equilibrium, whereas, when conditioned on $\langle \phi''^2 \rangle_r$, the degree of nonequilibrium of the conditional inertial-range scalar increases with $\langle \phi''^2 \rangle_r$. These results provide further evidence that the close-to-Gaussian conditional increment PDFs are a result of quasi-equilibrium scalar fields as implied in Kolmogorov's refined hypothesis, and suggests that the bimodal conditional FDFs are closely related to the nonequilibrium of the conditional inertial-range scalar.

To quantify the dependence of the conditional PDFs on the degree of nonequilibrium, we computed the bimodality parameter[18], $B = K - S^2$, as a function of $\langle \phi''^2 \rangle_r / \chi_r$ for three $\langle \phi''^2 \rangle_r$ values. Figure 13 shows that B is approximately independent of $\langle \phi''^2 \rangle_r$ and is largely a function of $\langle \phi''^2 \rangle_r / \chi_r$ alone. Therefore, the conditional PDF is largely determined by the degree of nonequilibrium. For

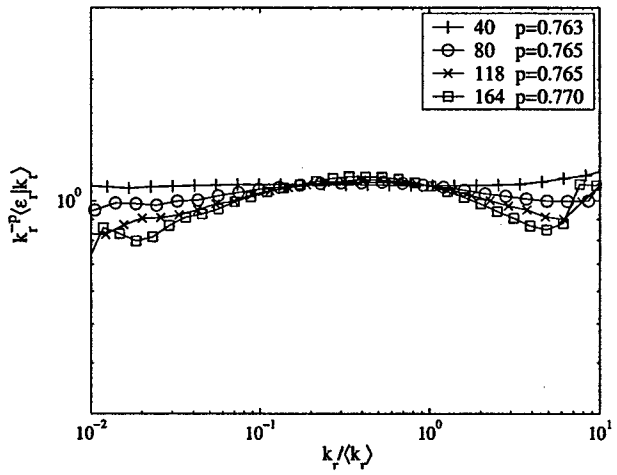

Figure 14: Conditional mean of the locally averaged energy dissipation $\langle\epsilon_r|k_r\rangle$ multiplied by k_r^{-p}, where p is the scaling exponent of $\langle\epsilon_r|k_r\rangle$. Approximate scaling ranges exist for all averaging domain sizes (given in the legend).

large $\langle\phi''^2\rangle_r/\chi_r$ values B appears to decrease monotonically towards unity (the slight increase of B for very large $\langle\phi''^2\rangle_r/\chi_r$ is due to insufficient statistical convergence there), indicating that the conditional increment PDF approaches a double delta function for strong nonequilibrium local scalar fields. The results suggest that the degree of spectral nonequilibrium can be parameterized by the ratio $\langle\phi''^2\rangle_r/\chi_r$ for three $\langle\phi''^2\rangle_r$, which can be modeled in LES.

F. Issues of modeling the filtered energy and scalar dissipation rates

In the velocity-scalar FJDF approach, the filtered energy dissipation and the filtered scalar dissipation require modeling. The current practice uses the spectral equilibrium assumption and therefore are inconsistent with the results discussed above. We investigated the issues of their modeling.

We first examined the statistical relationship between k_r and ϵ_r. Using Kolmogorov's refined hypotheses[20], one can write $k_r = V_2\epsilon_r^{2/3}r^{2/3}$ for an inertial-range separation r, where V_2 is a universal stochastic variable independent of ϵ_r. Thus, the conditional mean $\langle k_r|\epsilon_r\rangle$ scales as $\epsilon_r^{2/3}$, which has been confirmed experimentally[22]. However, the scaling exponent for the reversed conditional mean, $\langle\epsilon_r|k_r\rangle \sim k_r^p$, does not follow the K62 prediction of $p = 3/2$[22] and thus is "anomalous". Here we obtained the scaling exponents p by multiplying k_r^{-p} to $\langle\epsilon_r|k_r\rangle$ to obtain a flat portion of the curve (Fig. 14). For $r/\eta = 40$, there is a clear scaling range between $k_r/\langle k_r\rangle = 0.01$ and 3 with a scaling exponent of 0.763. For larger separations there are approximate scaling ranges where the variations of $k_r^{-p}\langle\epsilon_r|k_r\rangle$ are within 30% of the peak values. The exponents obtained are between 0.765 and 0.77. We might expect that at higher Reynolds numbers more definitive

scaling regions will emerge for these separations as well.

A possible explanation for the deviations of the observed scaling exponent p from predictions of Kolmogorov's refined hypotheses is that the hypotheses are based on quasi-equilibrium inertial-range spectral energy transfer, that is, the dissipation balances (or is larger than) the spectral transfer. Under such conditions the local energy dissipation time k_r/ϵ_r scales as the local energy production (spectral transfer) time $r/k_r^{1/2}$. When ϵ_r is used as the conditioning variable, this quasi-equilibrium condition is likely to be satisfied because, for a given magnitude of energy dissipation, there generally is a corresponding amount of the spectral transfer. Thus $\langle k_r|\epsilon_r\rangle$ scales as $\epsilon_r^{2/3}r^{2/3}$, but the reverse scaling, $\langle \epsilon_r|k_r\rangle \sim k_r^{3/2}$, is not necessarily true because an increase in the spectral transfer near the scale r can result in large k_r and a non-equilibrium local velocity field with the dissipation lagging behind. The nonequilibrium spectral transfer results in a slower increase of ϵ_r than the equilibrium prediction of $\epsilon_r \sim k_r^{3/2}$. In fact, the observed scaling $\epsilon_r \sim k_r^p$ shows that the ratio of the local energy dissipation time scale to the local production time scale varies as $k_r^{3/2-p}/r$, which increases with k_r. Thus, it appears that the anomalous scaling is due to the non-equilibrium of the local velocity fields. The results show that models for ϵ_L must take into account the nonequilibrium spectral transfer.

Next, we examined the issue of modeling χ_L. To understand the variations of the degree of non-equilibrium of the local scalar fields, it is useful to examine the relationship between $\langle\phi''^2\rangle_r$ and χ_r. In Fig. 15 we plot two conditional means, $\langle\langle\phi''^2\rangle_r|\chi_r\rangle$ and $\langle\chi_r|\langle\phi''^2\rangle_r\rangle$. The former increases as χ_r (the results are similar when $\chi_r\epsilon_r^{-1/3}$ is used as the conditioning variable), consistent with the K62 prediction

$$\langle\phi''^2\rangle_r = V_{\phi 2}\chi_r\epsilon_r^{-1/3}r^{2/3}, \tag{13}$$

where $V_{\phi 2}$ is also a universal stochastic variable independent of both χ_r and ϵ_r. However, the latter (as well as $\langle\chi_r\epsilon_r^{-1/3}|\langle\phi''^2\rangle_r\rangle$, not shown) scales approximately as $\langle\phi''^2\rangle_r^{0.7}$; therefore it is at variance with the K62 prediction of $\sim \langle\phi''^2\rangle_r$. A possible reason for the deviation of $\langle\chi_r|\langle\phi''^2\rangle_r\rangle$ from the K62 scaling is that the conditional inertial-range scalar is in quasi-equilibrium when conditioned on χ_r, whereas, when conditioned on $\langle\phi''^2\rangle_r$ it can be in nonequilibrium: For a given value of χ_r there generally is a corresponding amount of spectral transfer (scales as $\langle\phi''^2\rangle_r/\tau_{\phi r}$). Therefore, the scalar is in quasi-equilibrium. On the other hand, when $\langle\phi''^2\rangle_r$ (therefore the spectral transfer) is increased, χ_r generally lags behind since it takes time for the increased spectral transfer rate to reach the dissipation scales, resulting in non-equilibrium local scalar fields and a smaller scaling exponent for $\langle\chi_r|\langle\phi''^2\rangle_r\rangle$. Therefore, models for χ_L must contain the effects of spectral nonequilibrium.

The influence of the velocity field is also important for modeling χ_L and $\langle\phi''^2\rangle_L$ (the latter is needed in non-PDF-based LES) and was examined. The conditional mean of $\langle\phi''^2\rangle_L$ conditional on the filtered energy dissipation $\epsilon_L \equiv \langle\epsilon\rangle_L$ and the SGS energy, $\langle\langle\phi''^2\rangle_L|\epsilon_L, k_L\rangle$, is given in Fig. 16(a).

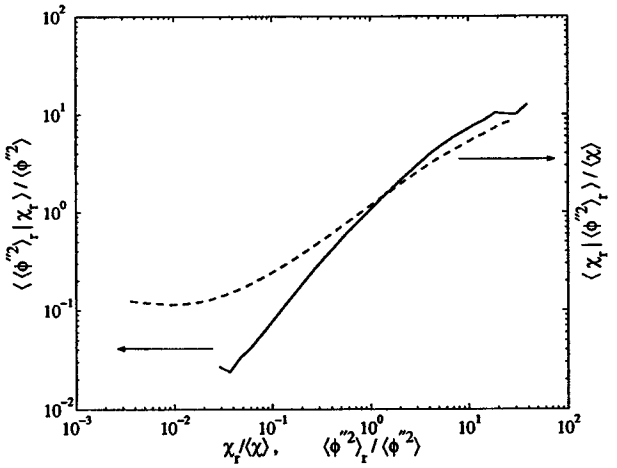

Figure 15: Conditional mean of the locally averaged scalar dissipation $\langle\langle\phi''^2\rangle_r|\chi_r\rangle$ and the reversed conditional mean $\langle\chi_r|\langle\phi''^2\rangle_r\rangle$.

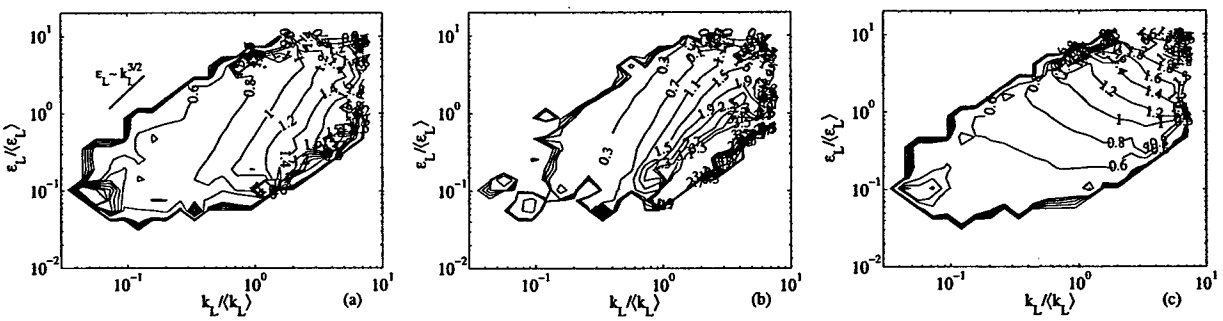

Figure 16: Conditional SGS scalar variance (a), SGS variance production (b), and filtered dissipation rate (c) conditional on ϵ_L and k_L.

The results with sufficient statistical convergence are limited to an elliptic region that approximately corresponds to the isocontours of the $\epsilon_L - k_L$ JPDF[21]. At $\epsilon_L/\langle\epsilon\rangle = 1$ and $k_L/\langle k_L\rangle = 1$ the SGS variance is close to its mean value ($\langle\langle\phi''^2\rangle_L|\epsilon_L, k_L\rangle = 0.9\langle\phi''^2\rangle$), indicating that the SGS scalar is close to its average conditions. Toward the lower right portion of the $\epsilon_L - k_L$ plane the SGS variance increases.

To understand this trend we computed the conditional means of the SGS variance production, $\langle P_{\phi L}|\epsilon_L, k_L\rangle$. The result given in Fig. 16(b) is normalized by $\langle\chi_{1L}|\epsilon_L, k_L\rangle$ and therefore represents the balance between the production and dissipation and the degree of nonequilibrium of the SGS scalar. Similar to the SGS variance, the production also increases toward the lower right portion of the $\epsilon_L - k_L$ plane. In addition, the isocontours have approximately the same slopes as those of $\langle\langle\phi''^2\rangle_L|\epsilon_L, k_L\rangle$, suggesting that $\langle\langle\phi''^2\rangle_L|\epsilon_L, k_L\rangle$ is largely determined by the degree of non-equilibrium of the SGS scalar and increases with it.

The conditionally filtered scalar dissipation rate, $\langle \chi_{1L} | \epsilon_L, k_L \rangle$, has isocontours approximately perpendicular to those of $\langle \langle \phi''^2 \rangle_L | \epsilon_L, k_L \rangle$ [Fig. 16(c)]. Therefore, χ_{1L} changes the fastest when the degree of nonequilibrium of the SGS scalar is held constant (along the isocontours of $\langle \langle \phi''^2 \rangle_L | \epsilon_L, k_L \rangle$ and $\langle P_{\phi L} | \epsilon_L, k_L \rangle$). For quasi-equilibrium spectral transfer, the filtered dissipation scales as $\chi_L \sim \langle \phi''^2 \rangle_L / \tau_{\phi L}$, where $\tau_{\phi L}$ is the SGS scalar time scale. Therefore, Fig. 16(c) suggests that the increase of χ_{1L} along the isocontours of $\langle \phi''^2 \rangle_L$ is due to the decrease in $\tau_{\phi L}$ caused by the velocity field. The results in Figs. 16(b) & (c) suggest that the SGS velocity causes $\langle \phi''^2 \rangle_L$ and χ_{1L} to increase by increasing the degree of non-equilibrium of the SGS scalar and by decreasing the SGS scalar time scale, respectively.

To further examine the effects of the velocity field, we considered the equilibrium property of the velocity field. A measure of the degree of nonequilibrium of the SGS velocity, which can be obtained from the data, is the conditional production of the SGS energy $\langle P_L | k_L, \epsilon_L \rangle / \epsilon_L$, where $P_L = -(\langle u_1 u_i \rangle_L - \langle u_1 \rangle_L \langle u_i \rangle_L) \partial u_i / \partial x_1$, $i = 1$ and 2. The isocontours of P_L (not shown) in the region $k_L > \langle k_L \rangle$ have slopes similar to those of $\langle P_{\phi L} | k_L, \epsilon_L \rangle / \chi_{1L}$. The results suggest that the observed trends for $\langle \langle \phi''^2 \rangle_L | \epsilon_L, k_L \rangle$ and $\langle \chi_{1L} | \epsilon_L, k_L \rangle$ are largely related to the degree of nonequilibrium and the time scale of the SGS velocity. Therefore, the velocity affects $\langle \langle \phi''^2 \rangle_L | \epsilon_L, k_L \rangle$ and $\langle \chi_{1L} | \epsilon_L, k_L \rangle$ through different processes that appear to have "orthogonal" effects.

These results have implications for SGS modeling. The filtered scalar dissipation has been modeled by assuming local equilibrium $\chi_L = P_{\phi L}$[23]. Figure 16(b) suggests that the model can be improved by including ϵ_L and k_L to account for the departure from equilibrium spectral transfer. The production $P_{\phi L}$ is available in velocity-scalar FJDF calculations and can be used to model χ_L. In addition, for LES that solves scalar transport equations, $P_{\phi L}/\chi_L$ can be modeled using $\langle \langle \phi''^2 \rangle_L | \epsilon_L, k_L \rangle$ and a scalar time scale determined by ϵ_L and k_L. The results for $\langle \langle \phi''^2 \rangle_L | \epsilon_L, k_L \rangle$ can also be used to test models for $\langle \phi''^2 \rangle_L$.

G. Preliminary study of the SGS mixing of the mixture fraction and the SGS flame structure in turbulent flames

Using the knowledge of SGS mixing gained in non-reacting flows we began to conduct a preliminary study of the mixture fraction filtered mass density function (FMDF), the SGS mixture fraction structure, and their influences on the SGS flame structure in turbulent flames. Experimental data obtained in Sandia flames D and E by Karpetis and Barlow (www.ca.sandia.gov/TNF/abstract.html) were used to analyze the SGS mixture fraction and the flame structure. One-dimensional filtering in the radial direction on data segments was employed to compute the FMDF and other resolvable-scale and subgrid-scale variables.

Conditional FMDF conditional on the Favre-filtered scalar (mixture fraction) and SGS scalar

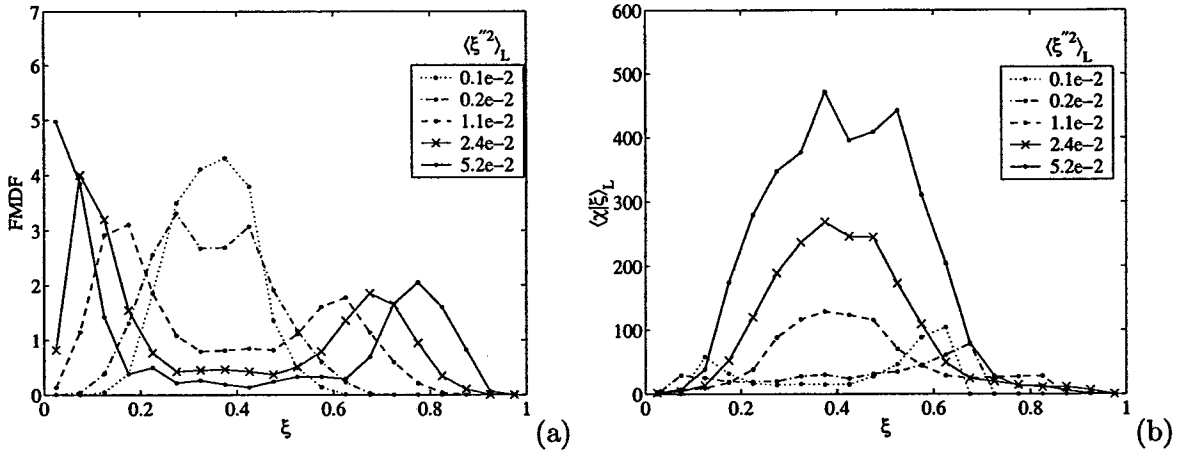

Figure 17: The mean conditional scalar FMDF (a) and the mean conditionally filtered scalar dissipation (b) obtained in Sandia flame D at x/D=15 with a filter size of $\Delta = 3.0mm$. The filtered mixture fraction $\langle\xi\rangle_L$ is set to the stoichiometric mixture faction, ξ_s, and the SGS variance values $\langle\xi''^2\rangle_L$ are given in the legend. Both the FMDF and the conditionally filtered scalar dissipation indicate qualitatively different SGS mixing regimes and SGS mixture fraction structure for small and large variance values.

variance shows a similar trend to the non-reacting results. For SGS scalar variance small compared to its mean, the FMDF is not far from Gaussian, and the conditionally filtered scalar dissipation rate depends weakly on the SGS scalar, indicating that the SGS scalar is well mixed (Fig. 17). For large SGS variance, however, the FMDF becomes bimodal, and the conditionally filtered scalar dissipation is bell-shaped, indicating the existence of a diffusion (dissipation) layer structure that is similar to the mixture fraction profile in the counter-flow model for laminar flamelets. For the measurement locations considered (up to 30 jet diameters downstream) the difference in mixture fraction values for the two FMDF peaks is generally larger than the reaction zone width in the mixture fraction space, and therefore the mixing field under such conditions can support flamelets. The conditionally filtered temperature near the stoichiometric mixture fraction decreases progressively with increasing SGS scalar variance. Furthermore, local extinction events appear to occur mostly when the SGS scalar variance is large, suggesting the possibility of flamelet extinction. These preliminary results suggest that the mixing regimes and the associated mixture fraction structure could potentially have a strong impact on the combustion regime and extinction/reignition in turbulent nonpremixed flames.

IV Conclusions and suggestions for LES

The results obtained in this research significantly advanced the understanding of the SGS velocity and scalar, which is important for modeling SGS mixing in LES of turbulent combustion. The issues include the velocity VFJDF and velocity-scalar FJDF, the structure of the SGS velocity

and scalar, the FJDF transport equation, and the filtered energy and scalar dissipation rates. The specific conclusions and suggestions for LES are:

- The velocity-scalar FJDF shows two mixing regimes: the equilibrium spectral transfer regime with close-to-Gaussian velocity and scalar FJDFs, and the nonequilibrium regime with bimodal scalar FDF and uniform velocity FJDF. The velocity-scalar structure in the nonequilibrium regime is similar to that of a laminar flamelet model. Therefore, consistency of mixing models with the flamelet limit is important.

- The velocity FJDF shows that the SGS turbulence is under local rapid distortion when the SGS velocity is in nonequilibrium. Eddy viscosity models (or when an eddy viscosity is implied) are inconsistent with local rapid distortion because the evolution of turbulence under rapid distortion is determined by the amount of strain, not the strain rate. The velocity-wavevector PDF model of Slooten and Pope[24] could be adapted to LES to model the local rapid distortion. However, this model may significantly increase the computational cost.

- The velocity-scalar FJDF and the dependence of the conditionally filtered scalar dissipation and diffusion on the SGS velocity further demonstrate the need to include velocity information in mixing models (e.g., the velocity conditioned model of Fox[25]). Currently employed mixing models are generally independent of the velocity.

- The degree of spectral nonequilibrium can largely be characterized and potentially parameterized by the SGS scalar variance and filtered scalar dissipation for the SGS scalar and by the SGS kinetic energy and the filtered energy dissipation rate for the SGS velocity. Therefore, LES contains the essential information to model the degree of nonequilibrium.

  The results also show that, contrary to Kolmogorov's refined hypotheses, the filtered dissipation χ_L and ϵ_L alone are not sufficient to describe the SGS scalar and velocity because the hypotheses are based on equilibrium spectral transfer.

- The filtered scalar and energy dissipation rates cannot be modeled accurately using the spectral equilibrium assumption. Nonequilibrium effects must be considered. The velocity field affects the SGS scalar variance and filtered scalar dissipation primarily by altering the degree of spectral nonequilibrium and the SGS time scale of the scalar, respectively. The effects can be parameterized by the SGS kinetic energy and the filtered energy dissipation rate. Therefore, the models for the SGS scalar variance and filtered scalar dissipation can be further improved by including the effects of the SGS kinetic energy and the filtered energy dissipation rate.

In collaboration with Professors Pope, Givi, and Pitsch we are currently working on testing models and LES predictions (FDF, etc.) and are exploring the possibilities of using the above suggestions to improve models. For example, the measured SGS mixing time increases with the SGS variance, whereas that used in the model does not. This model behavior does not allow the SGS variance in LES to fluctuate to the large values observed in the experiments. In addition, the conditional mixture fraction FMDF obtained in LES appears to have the bimodal shape at SGS variance values much larger than those in the experiments. These model behaviors may have a strong influence on the predicted reaction zone structure and will be addressed. Further activities in this area will be included in future project reports.

References

[1] S. B. Pope, "Computations of turbulent combustion: Progress and challenges," in *Proceedings of the 23rd Symposium (International) on Combustion* (1990), pp. 591–612.

[2] L. Y. M. Gicquel, P. Givi, F. A. Jaberi, and S. B. Pope, "Velocity filtered density function for large eddy simulation of turbulent flows," Phys. Fluids **14,** 1196–1213 (2002).

[3] M. R. H. Sheikhi, T. G. Drozda, P. Givi, and S. B. Pope, "Velocity-scalar filtered density function for large eddy simulation of turbulent flows," Phys. Fluids **15,** 2321–2337 (2003).

[4] C. Tong, "Measurements of conserved scalar filtered density function in a turbulent jet," Phys. Fluids **13,** 2923–2937 (2001).

[5] D. Wang and C. Tong, "Conditionally filtered scalar dissipation, scalar diffusion, and velocity in a turbulent jet," Phys. Fluids **14,** 2170–2185 (2002).

[6] A. G. Rajagopalan and C. Tong, "Experimental investigation of scalar-scalar-dissipation filtered joint density function and its transport equation," Phys. Fluids **15,** 227–244 (2003).

[7] S. B. Pope, "PDF methods for turbulent reacting flows," Prog. Eng. Combust. Sci **11,** 119–192 (1985).

[8] D. C. Haworth and S. B. Pope, "A generalized Langevin model for turbulent flows," Phys. Fluids **29,** 387–405 (1986).

[9] C. Speziale, "Galilean invariance of subgrid-scale stress in the large-eddy simulation of turbulence," J. Fluid Mech. **156,** 55–62 (1985).

[10] S. Tavoularis and S. Corrsin, "Experiments in nearly homogeneous turbulent shear flow with a uniform mean temperature gradient. Part 2. The fine structure," J. Fluid Mech. **104,** 349–(1981).

[11] K. S. Venkataramani, N. K. Tutu, and R. Chevray, "Probability distributions in a round turbulent jet," Phys. Fluids **18,** 1413–1420 (1975).

[12] V. Eswaran and S. B. Pope, "Direct numerical simulations of the turbulent mixing of a passive scalar," Phys. Fluids **31,** 506–520 (1988).

[13] R. S. Miller, S. H. Frankel, C. K. Madnia, and P. Givi, "Johnson-Edgeworth translation for probability modeling of binary mixing in turbulent flows," Combust. Sci. Tech. **91,** 21–52 (1993).

[14] C. Tong and Z. Warhaft, "Scalar dispersion and mixing in a jet," J. Fluid Mech. **292,** 1–38 (1995).

[15] M. R. Overholt and S. B. Pope, "Direct numerical simulation of a passive scalar with imposed mean gradient in isotropic turbulence," Phys. Fluids **8,** 3128–3148 (1996).

[16] P. Vedula and P. K. Yeung, "Similarity scaling of acceleration and pressure statistics in numerical simulations of isotropic turbulence," Phys. Fluids **11,** 1208–1220 (1999).

[17] S. Liu, J. Katz, and C. Meneveau, "Evolution and modeling of subgrid scales during rapid distortion of turbulence," J. Fluid Mech. **387,** 281–320 (1999).

[18] A. R. Masri, R. W. Dibble, and R. S. Barlow, "The structure of turbulent nonpremixed flames revealed by Raman-Rayleigh-LIF measurements,," Prog. Eng. Combust. Sci. **22,** 307 (1996).

[19] H. Zhang and C. Tong, "On conditional velocity increment statistics," Phys. Fluids **15,** 1676–1686 (2003).

[20] A. N. Kolmogorov, "A refinement of previous hypothesis concerning the local structure of turbulence in a viscous incompressible fluid at high Reynolds number," J. Fluid Mech. **13,** 82–85 (1962).

[21] D. Wang, C. Tong, and S. B. Pope, "Experimental study of velocity filtered joint density function and its transport equation," Phys. Fluids **16,** 3599–3613 (2004).

[22] C. Meneveau and J. O'Neil, "Scaling laws of the dissipation rate of the turbulent subgrid-scale kinetic energy," Phys. Rev. E **49,** 2866–2874 (1994).

[23] C. D. Pierce and P. Moin, "A dynamic model for subgrid-scale variance and dissipation rate of a conserved scalar," Phys. Fluids **10,** 3041–3044 (1998).

[24] P. R. Van Slooten and S. B. Pope, "PDF modeling for inhomogeneous turbulence with exact representation of rapid distortions," Phys. Fluids 9 (1997).

[25] R. O. Fox, "On velocity-conditioned scalar mixing in homogeneous turbulence," Phys. Fluids **8,** 2678–2691 (1996).

Publications resulted from this research

1. Wang, D. and Tong, C. 2005 Experimental study of velocity-scalar filtered joint density function for LES of turbulent combustion. *Proc. Combust. Inst.* **30**, 567–574.

2. Wang, D, Tong, C. and Pope, S. B. 2004 Experimental investigation of velocity-scalar filtered density function for large eddy simulation. *Phys. Fluids* **16**, 3599–3613.

3. Zhang, H., Wang, D, and Tong, C. 2004 On conditional scalar increment and joint velocity-scalar increment statistics. *New J. Phys.* **6** (Focus issue on turbulence), 38.

4. Zhang, H. and Tong, C. 2003 On conditional velocity-increment statistics. *Phys. Fluids* **15**, 1676–1686.

5. Tong, C. 2003 Galilean invariance of velocity probability density function transport equation. *Phys. Fluids* **15** 2073–2076.

Presentations on the results from this research

1. Investigation of scalar filtered mass density function in turbulent partially premixed flames. The Fourth Joint Meeting of the US sections of the Combustion Institute. Philadelphia, March 2005.

2. Experimental study of velocity-scalar filtered joint density function for large-eddy simulation of turbulent combustion. The Fifty-Seventh Annual Meeting of the Division of Fluid Dynamics of the American Physical Society. Seattle, November 2004.

3. On joint conditional velocity-scalar increment statistics. The Fifty-seventh Annual Meeting of the Division of Fluid Dynamics of the American Physical Society. Seattle, November 2004.

4. Seminar, Center for Environmental and Applied Fluid Mechanics Seminar, Johns Hopkins University. November 2004.

5. Experimental study of velocity-scalar filtered joint density function for large-eddy simulation of turbulent combustion. The Thirty First International Symposium on Combustion. Chicago, July 2004.

6. Seminar, Center for Turbulence Research Seminar, Stanford University. May 2004.

7. Experimental study of velocity filtered joint density function and its transport equation for large-eddy simulation. The Third Joint Meeting of the US sections of the Combustion Institute. Chicago, March 2004.

8. Experimental study of subgrid-scale velocity-scalar distribution. The Fifty-sixth Annual Meeting of the Division of Fluid Dynamics of the American Physical Society. New Jersey, 2003.

9. On conditional scalar increment statistics. The Fifty-sixth Annual Meeting of the Division of Fluid Dynamics of the American Physical Society. New Jersey, 2003.

Participating Personnel

Chenning Tong: Assistant Professor (4/1/2002-6/30/2005)

Danhong Wang: Graduate student (8/15/2002-3/31/2005. Ph.D., August 2005)

Hengbin Zhang: Graduate student (4/1/2002-8/14/2002)

Interactions with researchers at AFRL

During the period of this grant, the PI initiated contacts with several researchers at AFRL to seek opportunities for collaborations. Potential topics of collaborations were identified as a result of the subsequent discussions with the researchers. In particular, the discussions with Dr. Campbell Carter initiated by the PI in 2004 resulted in a collaborative project. In the summer of 2005, the PI spent several weeks at AFRL as part of the collaboration.

This collaboration focuses primarily on issues of using measurements to improve of large eddy simulation (LES) of nonpremixed turbulent combustion. In PDF-based LES approaches the subgrid-scale mixing of multiple scalars must be modeled. Current mixing models are based primarily on knowledge gained from two-stream mixing problems (e.g., fuel mixing with oxidizer). However, in a reacting flow at least three scalars are involved (the third is a product). Therefore, understanding of three-stream SGS mixing is important for modeling mixing in nonpremixed turbulent combustion. As a step toward understanding SGS mixing of multiple reactive scalars, the PI and Dr. Carter will study the SGS mixing in a three-stream non-reacting jet. The jet nozzle consists of an axisymmetric jet and an annulus from which acetone-doped air and ethylene are issued into an air co-flow. Laser diagnostics (planar laser induced fluorescence and Rayleigh scattering) are employed to obtain images of the species. This study will provide a basis for future investigations of multi-scalar SGS mixing in turbulent flames.

Inventions

None